Chaotic Stirring in a Tidal System

H. Ridderinkhof and J. T. F. Zimmerman

An analysis of a two-dimensional tidal model of the Wadden Sea reveals Lagrangian chaos in the trajectories of water parcels. The associated chaotic stirring results from the transverse intersection of the stable and unstable curves of hyperbolic fixed points in the Lagrangian residual displacement field (the tidal Poincaré map). This tidal dispersion mechanism produces rapid water exchange along the channel axis and could be representative of many shallow tidal seas.

Mixing or dispersion in tidal basins is an extremely complicated process (*1, 2*). It affects all biotic and abiotic substances dissolved or suspended in the water. In particular, it determines to a large extent the time scales of homogenization inside the basin and of the flushing of the adjacent continental shelf with external water masses. The traditional view is to regard the effective horizontal dispersion as an interaction of turbulence generated by the tidal currents at the sea bed and the horizontal or vertical shear of these currents. The turbulence proper introduces a random walk of the water parcels, amplified by its interaction with the shear. In this way, horizontal dispersion coefficients up to 100 $m^2 s^{-1}$ can be reached if the shear is uniform over distances of the tidal excursion amplitude (on the order of 10 km) and the turbulent mixing time scale over the shear width is much smaller than the tidal period (*2, 3*). In many tidal areas, however, the horizontal shear pattern is extremely irregular over length scales less than the tidal excursion. On the other hand, these length scales are large enough to have horizontal, turbulent mixing time scales in excess of the tidal period. Thus, there is sufficient reason to doubt whether turbulent shear dispersion is the principal mixing process in shallow tidal embayments (*2*).

There are, however, other possible ways to produce dispersion (that is, randomization of particle trajectories) in tidal flows with irregular horizontal structures. Zimmerman (*4*) proposed that the necessary randomization could be achieved without the recourse of small-scale turbulence if one regards the tidal velocity field as an oscillatory current superimposed on a pattern of (time-independent) residual currents that are a random function of position only. These residuals are generated by the tide itself in interaction with the irregular bottom topography and are often organized in eddy-like structures (*5*). The superposition then leads to a "tidal random walk" (*4*), the properties of which can be used to quantify a dispersion coefficient that is controlled by two dimensionless parameters: (i) λ, the ratio of the tidal excursion to the residual eddy diameter, and (ii) v, the ratio of the residual velocity to the tidal velocity. Dispersion is optimal for λ values of order unity [0 (1)] (*2*).

Recently, however, it has become evident that randomness of the (Eulerian) velocity field is not necessary to have (Lagrangian) trajectories of water parcels that are random functions of time. The phenomenon has been observed in a host of laboratory and numerical experiments in various fluids (*6, 7*) and plasmas (*8*), particularly in two-dimensional (2-D) time-periodic flows. The clue to this behavior is that for a given 2-D time-periodic velocity field, the equations for the (Lagrangian) particle velocities are analogous to the Hamiltonian equations of motion of a dynamical system with one and a half degrees of freedom, with the stream function of the prescribed field acting as the Hamiltonian. Under certain conditions the motion in the phase space, spanned by the canonical coordinates of the Hamiltonian (which are the physical coordinates in a 2-D fluid), can be chaotic (*6, 9*). Thus, in time-periodic 2-D fluids, the trajectories can also be chaotic. This Lagrangian chaos is volume (or area) conserving and therefore only a complicated stirring process (*10*) (chaotic stirring). However, the fluid may have mixing properties in a coarse-grained sense (*11*) even though the Eulerian velocity field is completely nonturbulent and deterministic. Moreover, the generic type of flow in these systems is such that not all trajectories are chaotic but that the phase space is covered with coherent areas (islands), from which particles cannot escape (*12*). Together,

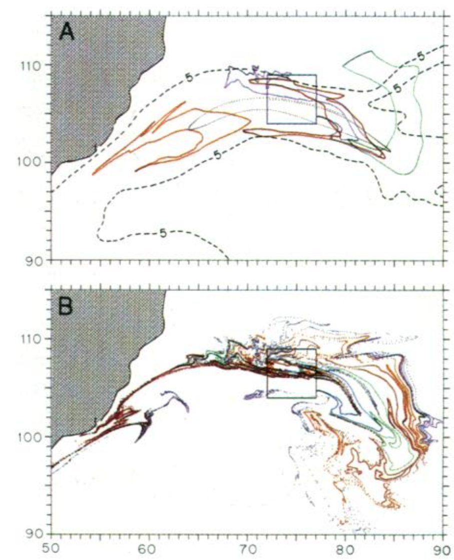

Fig. 2. (**A**) The distortion of an initially rectangular array of particles during the first tidal cycle (blue), after 0.25 period (orange), 0.5 period (red), 0.75 period (green), and 1 period (violet). The tidal excursion of a single particle is shown by the dotted black line. The 5-m isobath marks the direction of the tidal channel. Each grid unit is 500 m. (**B**) As (A) but now after 1 (blue), 2 (green), 3 (red), 4 (orange), and 5 (violet) tidal cycles.

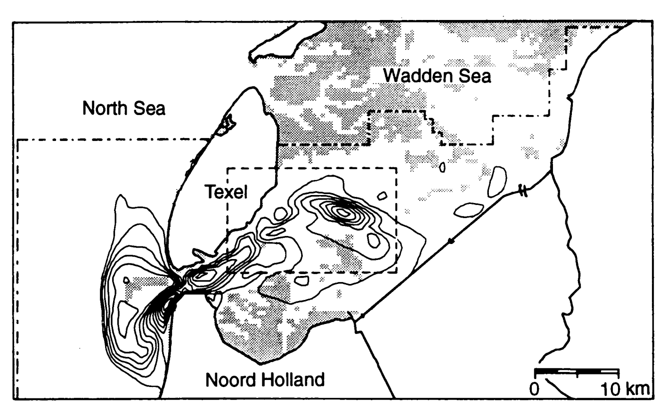

Fig. 1. The western Dutch Wadden Sea. The part enclosed by the dashed-dotted line and the coastline marks the boundary of the numerical model (*34*) that was used to simulate the vertically averaged tidal currents in the area. The model reproduces the spatial structure of the velocity field of the principal semidiurnal lunar tide, M_2, and all its harmonics ($M_{4,6,...}$), and of the rectified residual component, M_0. The $M_{2,4,6}$ components are prescribed at the open boundary of the model and propagate into the area. The harmonics and the residual are also generated internally by nonlinear processes. The residual circulation cells are shown by their streamlines. They agree well with observations from current meter measurements (*4*). Tidal flats are shaded. The dashed rectangle in the center is the principal area of investigation.

H. Ridderinkhof is at the Netherlands Institute of Sea Research, Post Office Box 59, 1790 AB Texel, the Netherlands. J. T. F. Zimmerman is at the Netherlands Institute of Sea Research and the Institute of Marine and Atmospheric Research, Utrecht University, Utrecht, the Netherlands.

these islands could be identical to the patchiness that is sometimes observed in drifter experiments (13) and in the distribution of various substances in the sea. Chaotic stirring in time-periodic flows can therefore be an effective horizontal dispersion process in tidal areas (2, 14, 15). Indeed it has appeared that the control parameters, λ and v, of the tidal random-walk model (4) are precisely the same as those determining the appearance of Lagrangian chaos in numerical experiments (16). There are also indications that the effective dispersion by chaotic stirring exhibits a resonance (8, 17) for $\lambda \approx 0$ (1).

Guided by these observations, we looked for the appearance of Lagrangian chaos in a realistic, 2-D numerical model of one of the best investigated areas with strong tidal mixing, the Dutch Wadden Sea. We first show some of the indications of chaos in the particle trajectories of the model. Then we discuss the characteristics of Lagrangian chaos in a simple dynamical system representative of the flow in a complicated tidal basin, the properties of which resemble those of chaos in periodically perturbed traveling waves (18). Finally, we revisit the model of the Wadden Sea to demonstrate unequivocally the existence of chaotic stirring and its importance as a mixing process.

Particle Spreading in a Model of the Wadden Sea

The Wadden Sea is a tidal area of extreme geomorphological complexity, located behind a chain of islands off the Dutch, German, and Danish coasts (19). Each separate basin is connected to the North Sea by a tidal inlet 5 to 10 km wide and more than 10 m deep. Inside the basin the inlet branches into several channels that drain a topographically complicated area of tidal flats. The tide cooscillates with that of the North Sea and is principally semidiurnal, with the lunar semidiurnal tide, M_2, as the dominant component. Vertical tidal ranges vary between 1.5 and 3 m, depending on the amplitude in the adjacent North Sea and the state of resonance of the basin concerned. In the middle of the deeper channels, vigorous tidal currents easily reach speeds of 1.5 m s^{-1}. The irregular bottom topography induces large spatial irregularities in the current velocity field, which is periodic in time everywhere (20) but a complicated function of position. Differential bottom friction and its associated vorticity dynamics (21) primarily cause this irregularity and the associated strong straining in the velocity field. Nonlinear vorticity advection is responsible for a "rectified" or "residual" current pattern that persists after the tidal current velocity has been averaged at each position over the tidal period. Analyses of current velocity measurements (4, 22) and numerical simulations (21) show the existence of residual eddies all over the area with current speeds up to 0.2 m s^{-1}.

To demonstrate the general features of particle spreading, we focus here on the central part of the western Dutch Wadden Sea (Fig. 1). First we show (Fig. 2) the deformation of an initially rectangular array (2.5 by 2.5 km) of particles in the central part of the area near one of the big residual eddies. The number of particles is 500 per grid unit of 500 m. We followed the fate of the rectangle first through a complete tidal cycle (Fig. 2A) and then, respectively, after two, three, four, and five tidal cycles. We also show (Fig. 2A) the trajectory of a single particle over a full tidal cycle to give an estimate of the tidal excursion amplitude, which was about 10 km here. A parcel traverses an area of the same extent as the residual eddy and therefore samples a spatially complicated part of the Eulerian velocity field. The results in Fig. 2A show that different particles sampled different parts of the velocity field and that this process created a strong and nonuniform stretching and folding of the initially rectangular array. In a single tidal cycle the rectangle was completely distorted and its perimeter grew considerably. This process was repeated during each tidal cycle thereafter (Fig. 2B). Already after two cycles have passed it is hard to reconstruct the perimeter, which has an irregular structure and extends far outside the area covered by the initial tidal excursion. Thus we see a real transport of material out of the bounds set by the tidal velocity field proper. Moreover, on closer inspection the length growth of the perimeter appears highly irregular. This behavior results only from the presence of a spatially complex, yet strictly time-periodic and deterministic, tidal velocity field. There were no turbulent velocities present and therefore there was no turbulent (shear) diffusion in the proper sense. Thus the volume enclosed by the stretched and folded perimeter was conserved. All of these properties—sensitivity of the trajectory to the initial position, folding and stretching of material areas, strong but irregular growth of the patch perimeter—indicate the presence of Lagrangian chaos and its importance as a transport process.

Particle Spreading in a Simple Model

The complicated tidal and residual velocity field in the Wadden Sea can be thought of as the superposition of many spatially periodic modes with different horizontal wave numbers produced by the interaction of bottom topography and the tides. Each wave number in the topography creates a component in the velocity field, the amplitude of which is a function of λ and the amplitude of the topographic component (5). For residual currents the response is largest if $\lambda \approx 0$ (1). Pasmanter (14) realized that, no matter how complicated the spatial structure of the superposition of all modes may be, even the presence of a single mode could give rise to chaos in the particle trajectories. We elaborated his model to illuminate the basic mechanisms of particle spreading.

Suppose that the (quasi–2-D) residual and tidal topographic velocity fields are derived from a 2-D, spatially periodic stream function $S(x,y)$ with the same wavelength in both directions, the strength of which is a strictly periodic function of time $T(t)$. This function forms a lattice of eddies upon which is superposed a spatially uniform, rectilinear tidal current of the same time periodicity. For given initial conditions (x_0, y_0) the particle trajectories $[x(t), y(t)]$ are then given by the solution of the system (23):

$$\dot{x} = u(x,y,t) = \lambda\{T(t) + v[1 + T(t)]S_y(x,y)\} \quad (1)$$

$$\dot{y} = v(x,y,t) = -\lambda[1 + t(T)]S_x(x,y) \quad (2)$$

where

$$T(t) = \cos(2\pi t) \quad (3)$$

and

$$S(x,y) = \frac{1}{\pi}\sin(\pi x)\sin(\pi y) \quad (4)$$

Evidently this model represents a nondivergent velocity field. Thus any initial area is conserved under evolution described in Eqs. 1 and 2. The parameters λ and v determine the quality of the solution, particularly the occurrence of chaos. For the sinusoidal functions $T(t)$ and $S(x,y)$ given in Eqs. 3 and 4, the trajectories can be found by numerical integration. However, to minimize numerical errors we adopted Pasmanter's (14) approach and replaced $T(t)$ with an alternating step function of unit period and $S(x,y)$ with a sawtooth function of double-unit wavelength in both coordinates. For each period of the oscillation, the solution can then be obtained by piece-wise analytical integration, and the coupled differential equations reduce to a mapping (24)

$$(x,y)_{n+1} = M[(x,y)_n] \quad (5)$$

where n is the iteration number, or the number of (tidal) periods.

After iteration over ten periods of 200 particles initially distributed evenly over an eddy cell ($x = 0,1$; $y = 0,1$), maxima in the particle variance in the x direction appear with approximately the same magnitude for

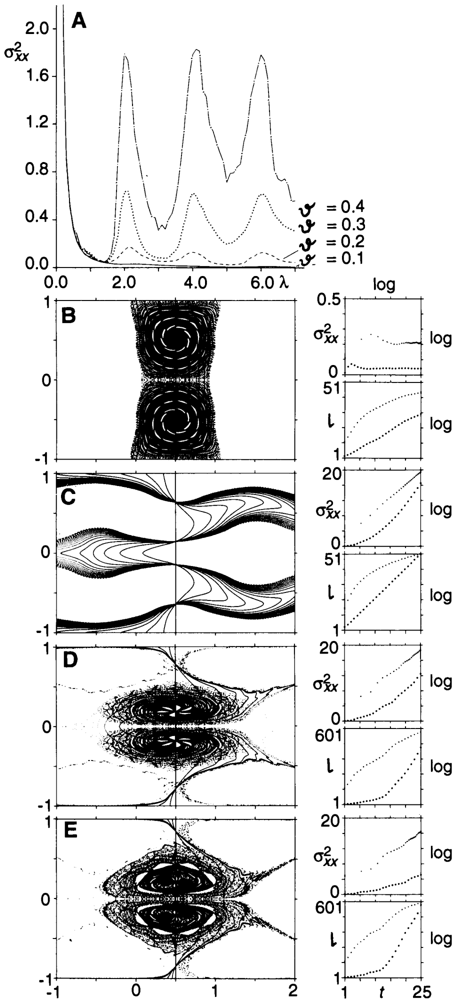

Fig. 3. (**A**) The x-variance, σ^2_{xx}, relative to the squared tidal excursion amplitude of 100 particles that were initially evenly distributed over a circulation cell, after 10 periods. Variance is given as a function of the ratio of the tidal excursion amplitude to the eddy diameter (λ) for different values of the ratio of eddy velocity to the tidal velocity (ν). For $\nu = 0.3$ and λ values (**B**) 1.5, (**C**) 2.0, (**D**) 2.5, and (**E**) 3.0, the distortion of a vertical line through the eddy cell is shown for (B) to (E) by a Poincaré section. On the right for each λ, (top) the x-variance of the particle displacement as a function of iteration number and (bottom) the length growth of the line element (ℓ), both linear (lower curve, large dots) and log-log (upper curve, small dots); time, t, in interaction number.

$\lambda = 2, 4, 6$ and minima for $\lambda = 1, 3, 5$ (Fig. 3A). There is a general increase of the spreading with ν. To interpret this behavior, we show in Fig. 3, B to E, for four values of λ a sequence of Poincaré sections by plotting 25 successive positions of 2000 particles. Initially, the particles were separated by equal distance on a line through the center of a circulation cell. The sequence has the following properties:

1) For $\lambda = 1.5$ (or smaller), all particles

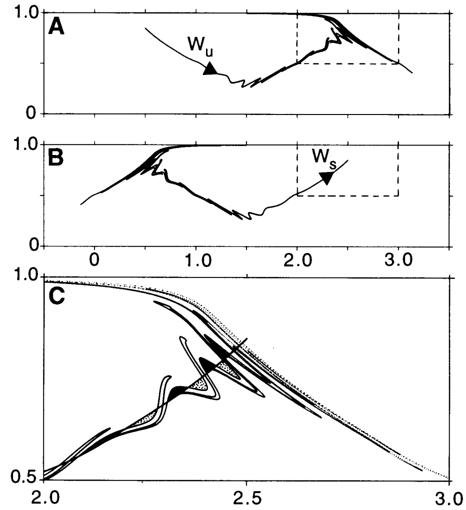

Fig. 4. Construction of the unstable (**A**) and stable (**B**) curves of, respectively, the hyperbolic fixed points at ($x = 0.5$, $y \approx 0.8$) and ($x = 2.5$, $y \approx 0.8$) for parameter values $\lambda = 3$ and $\nu = 0.2$. In (**C**) we show a magnification of the cadred area in (A) and (B). Successive equal areas of the iteration are shown dotted and black.

remain trapped in the circulation cell and rotate around elliptic points forming a "whorl" (*25*). After some time the growth of the x-variance stops and, more important, the growth of the initial line is exactly linear in time. The regime is not chaotic, and all particles tend to follow approximately the streamlines of the topographic circulation cell.

2) However, as soon as λ is raised above 1.5, particles appear to escape from the cell in both the negative and positive x directions and other particles remain trapped in islands. The size of these islands decreases with λ until, at $\lambda = 2$, all islands have disappeared and all particles travel in bands of alternating direction, so-called "advective channels." The variance in the x direction is now proportional to t^2, but the growth of a line element is still linear in time. Nonlinearity here creates a kind of Lagrangian shear flow but no chaos. The fixed points that separate the advective channels of different direction are parabolic. They are at the center line of the cells but not at the elliptic points of the cells proper.

3) When λ is now increased further (Fig. 3, D and E), islands of trapped particles, as well as the associated elliptic points, reappear, but hyperbolic points arise at $y \approx 0.8$. These mark the onset of chaos in the particle trajectories that is particularly clear in the line stretching that is now exponential rather than linear. The variance grows as $t^{1.7}$ (Fig. 3D) and $t^{1.5}$ (Fig. 3E), which indicates anomalous diffusion (*14, 18, 26*). This diffusion probably results from a mixture of trapped particles ($\sigma^2 \sim$ constant), particles still traveling in advective channels ($\sigma^2 \sim t^2$) and particles wandering chaotically over the area in a kind of random walk ($\sigma^2 \sim t$). The decrease of the number of particles traveling in the advective channels and the increase in the size of the islands if λ is raised from 2.5 to 3 are then reflected in the diminishing of the exponent from 1.7 to 1.5. Inside the trapping regions, chaotic areas may also exist. In this case a homogenization in these areas occurs, but the particles cannot escape the region inside the outermost closed invariant curve surrounding an island.

This sequence repeats itself for larger values of λ, as shown by the particle variance as a function of λ (Fig. 3A).

A definite conclusion about the appearance of chaotic trajectories can be obtained by a more detailed analysis of the hyperbolic fixed points in the Poincaré sections. To each hyperbolic point two stable and two unstable invariant curves are connected along which a particle proceeds to or recedes from the point exponentially slowly. If the stable and unstable curves of different hyperbolic points intersect, chaos sets in (*6, 9*). A general property of area-conserving maps is that the distance between successive intersection points becomes ever smaller and the unstable curve exhibits loops of ever-increasing length that transversely intersect the stable curve. The strong stretching and folding of this "tendril" (*25*) create chaotic stirring. This behavior also occurred in our results (Fig. 4). The extreme increase in stretching is immediately evident. Material is smeared out over large distances when the hyperbolic point is approached because the area between both curves is conserved. In the context of tidal mixing this behavior means that water exchange is strongly promoted near the hyperbolic points of a "tidal Poincaré map" once the governing parameters λ and ν have exceeded the critical values for the onset of chaos. The observational (*4, 22*) and numerical (*21*) evidence we have for the western Dutch Wadden Sea gives a range of λ for the residual eddies between 2 and 4 and of ν between 0.05 and 0.3. For the residual eddy in the central area of Fig. 1, the parameter values are $\lambda \approx 3.0$ and $\nu \approx 0.2$. Judging by the results of the simple model (*1, 2*), we must therefore expect signs of chaotic stirring in that area.

Revisiting the Wadden Sea Model

Because hyperbolic fixed points and the eventual transverse intersection of unstable and stable curves are the crucial properties of chaotic stirring, we now return to the numerical model of the Wadden Sea to determine whether we can locate these points and curves in the tidal Poincaré section of a part of the area. The Lagrangian residual velocity field (*27*) of a large number of grid points in the central part of the Wadden Sea (Fig. 5A) was obtained by calculation of the net displacement of each point over a tidal cycle, with all points starting at the same initial phase of the tide. In a sense, the field is a Poincaré section because each vector gives distance and direction over which the particle is displaced after one tidal period. We located three elliptic and two hyperbolic points in this region. Next we constructed the stable and unstable curves of two of the hyperbolic points that appear to intersect transversely (Fig. 5A). The result of this intersection is that fluid is strongly stretched parallel to the channel direction and compressed in the cross-channel direction to produce an appreciable longitudinal water exchange in the area.

These results are further illustrated (Fig. 5B) by examination of the effect of a hyperbolic and elliptic point on a line element that is initially located near the elliptic point. The line consists of 10^4 points. As soon as the initially upper segment approaches the western hyperbolic point, it undergoes a strong stretching and folding in the channel direction. This is a self-similar process (Fig. 5C) that also occurs on smaller scales. This indicates fractal structure in the line stretching, another property of chaotic stirring (*28*). On the other hand, most particles of the initially lower part of the line rotate around the elliptic point and seem to be trapped there. The behavior of the line stretching appears to be exponential with a Lyapunov exponent of order 1 (tidal period)$^{-1}$, but the stretching is irregular, probably because of the inhomogeneity of the flow.

After three tidal periods the density distribution of the points forming the initial line segment is such that there are multiple maxima and the spreading is predominantly along the channel axis (Fig. 6A). The first property is a clear indication that, although chaotic, the spreading certainly does not give rise to a Gaussian distribution and therefore it cannot be described by a simple random walk model. Although the assignment of a diffusion coefficient to this process is therefore dubious, the variance of the particle distribution after three tidal periods is equivalent to a longitudinal diffusion coefficient of the order 100 $m^2\ s^{-1}$, which is in the range of values observed in dye experiments in similar tidal areas (*29*). However, if we simulate the dispersion process in a random walk model with Fickian diffusion coefficients that give an overall spreading with a variance similar to the chaotic stirring model, then the multiple maxima disappear and the density distribution is much more homogeneous and approximately Gaussian (Fig. 6B). Nonetheless, because turbulent diffusion in all tidal areas always competes with other dispersion processes, one may well ask what its influence is on the "coarse-grained" distribution of Fig. 6A. Therefore, we have added to the chaotic stirring experiment a small-scale random walk equivalent to an isotropic, turbulent diffusion coefficient $D = 0.02uH$ (where u is the tidal velocity amplitude and H is the local water depth), representative of genuine horizontal turbulence in a tidal current (*2, 30*). It primarily gives a larger cross-channel dispersion (Fig. 6C), but the overall inhomogeneous distribution remains unaffected. However, in the long run turbulent diffusion destroys the lamellar structure of chaotic stirring. Probably this picture comes nearest to reality.

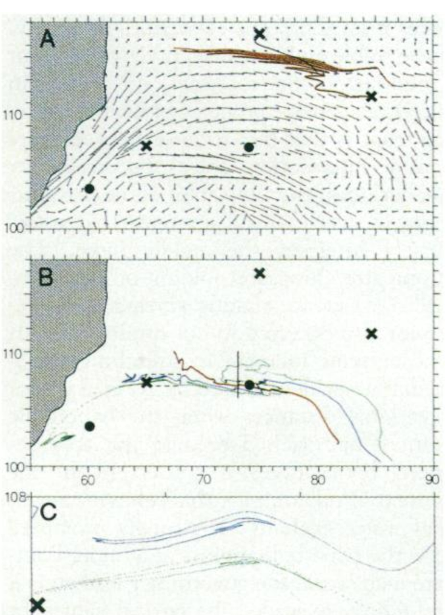

Fig. 5. (**A**) Lagrangian residual velocity field in the central part of the Wadden Sea calculated by numerical integration of a particle trajectory with the use of the Eulerian velocity field of our tidal model. A vector the size of one grid unit is equivalent to a residual velocity of 0.1 $m\ s^{-1}$ or to a residual displacement in the vector direction of 4.5 km (nine grid units). Hyperbolic (crosses) and elliptic (filled circles) fixed points are shown together with the stable (blue) and unstable (red) invariant curves of, respectively, the northern and eastern hyperbolic points. (**B**) Line stretching and folding of an initially straight line segment of 10^4 particles (black) near the central elliptic point after 1 (red), 2 (blue), and 3 (green) tidal periods. (**C**) Magnification of the dashed rectangle in (B) showing the self-similar structure of folding and stretching.

Conclusion

Although the Eulerian velocity field in the Wadden Sea is much more complicated than most of the laboratory or numerical models studied before, particle spreading appears to be qualitatively similar to chaotic stirring in simple deterministic time-periodic velocity fields of two dimensions. The stirring process is governed by the location of hyperbolic and elliptic fixed points in the tidal Poincaré map, but, because of the complex morphology, the distribution of these points over the area is irregular. In our simulations the dimensions of islands surrounding elliptic points appear to be much smaller than the chaotic regions, and advective channels could not be detected. Thus the large spreading of particles in the Wadden Sea can be attributed largely to the presence of hyperbolic fixed points and the transverse intersection of their associated invariant stable and unstable curves. The latter is the primary mechanism of water exchange that may probably be quantified by more careful analysis of the dynamics of the lobes (*31*). At large horizontal length scales, the process is not much affected by smaller scale turbulent

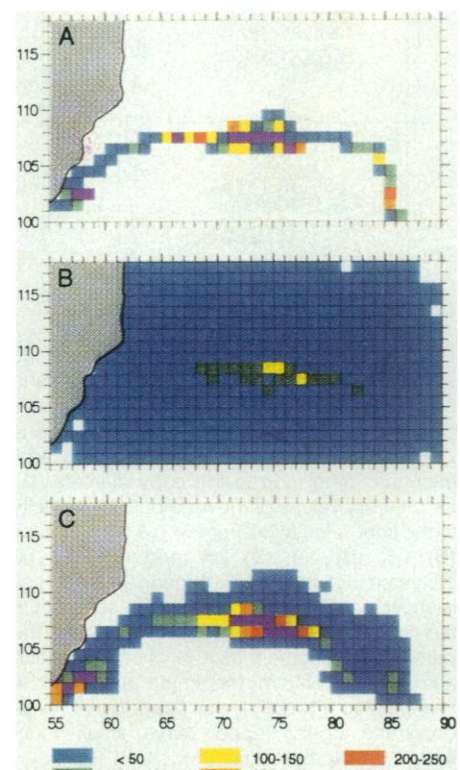

Fig. 6. (**A**) Particle distribution in numbers per grid unit of the line segment of Fig. 5, B to C, after 3 tidal periods when only the deterministic tidal velocity field is present. (**B**) As (A) without the tidal velocity field but with a random walk equivalent to diffusion in the along- and cross-channel directions. The coefficients are of the order 100 $u_{a,c}$ $m^2\ s^{-1}$, where u_a is the tidal velocity amplitude along the channel axis and u_c is the amplitude in the cross direction. (**C**) As (A) with a random walk superposed on the tidal velocity field equivalent to an isotropic, small-scale turbulent diffusion coefficient of the order $0.02uH$ $m^2\ s^{-1}$.

diffusion, although this process smooths the striations caused by chaotic stirring (*32*), which gives a more realistic distribution pattern on smaller length scales. Proper modeling of the deterministic tidal velocity field, particularly on the smaller horizontal length scales, is therefore of much more importance than a detailed modeling of the genuine turbulence. Under favorable conditions, once the deterministic tidal velocity field is sufficiently irregular in space, large-scale stirring by chaotic particle movements is already implied. This stirring can also account for the patchiness and multiple maxima in the concentration distribution of effluent from point discharges (*33*). This connection may explain why some parts of a tidal area are rapidly flushed but in others water seems to be stagnant for a longer time, keeping biological and chemical processes with a large reaction time scale viable against the always present dispersion processes. The process of chaotic stirring we have presented here seems generic in that it may occur in many tidal embayments worldwide where the bottom topography creates sufficient spatial complexity in the tidal current velocity field. Such stirring could be detected with the procedures described here by simulation of the tidal velocity field with a numerical model. This model would need sufficient spatial resolution, particularly of the bottom topography, and a proper representation of the nonlinear terms in the equations of motion.

REFERENCES AND NOTES

1. H. B. Fischer *et al.*, *Mixing in Inland and Coastal Waters* (Academic Press, New York, 1979); W. R. Geyer and R. P. Signell, *Estuaries* **15**, 97 (1992).
2. J. T. F. Zimmerman, *Neth. J. Sea Res.* **20**, 133 (1986).
3. Shear dispersion in oscillatory (tidal) currents was first treated in K. F. Bowden, *J. Fluid Mech.* **21**, 83 (1965); A. Okubo, *Int. J. Limnol. Oceanogr.* **1**, 194 (1967); *J. Oceanogr. Soc. Jpn.* **24**, 60 (1968). In a tidal area one may distinguish between horizontal diffusion by vertical shear and by horizontal shear, of both the oscillatory and residual parts of the current. With increasing width of an estuary or tidal inland sea, horizontal shear, particularly of the residual currents, rapidly becomes the dominant mechanism; see (*2*) and J. Dronkers and J. T. F. Zimmerman [*Oceanol. Acta Spec. Publ.*, p. 107 (1982)]. This is the main reason why, for large-scale dispersion, a vertically averaged 2-D model may be used, without regard to variations of current velocity with depth.
4. J. T. F. Zimmerman, *Neth. J. Sea Res.* **10**, 397 (1976).
5. _____, *Geophys. Astrophys. Fluid Dyn.* **11**, 35 (1978); *J. Mar. Res.* **38**, 601 (1980); *Nature* **290**, 549 (1981).
6. J. M. Ottino, *The Kinematics of Mixing: Stretching, Chaos and Transport* (Cambridge Univ. Press, Cambridge, 1989).
7. See reviews in: H. Aref *et al.*, *Physica D* **37**, 423 (1989); H. Aref, S. W. Jones, S. Mofina, I. Zawadzki, *Philos. Trans. R. Soc. London Ser. A* **333**, 273 (1991); V. V. Beloshapkin *et al.*, *Nature* **337**, 133 (1989); J. M. Ottino, in *Topological Fluid Mechanics*, H. K. Moffatt and A. Tsinober, Eds. (Cambridge Univ. Press, Cambridge, 1990), pp. 13–22; G. M. Zaslavsky *et al.*, *Weak Chaos and Quasi-Regular Patterns* (Cambridge Univ. Press, Cambridge, 1991); A. Crisanti *et al.*, *Riv. Nuovo Cim.* **14** (no. 12), 1 (1991); and the research notes of R. Pool [*Science* **250**, 627 (1990)] and S. Wiggins [*Nature* **333**, 395 (1988)].
8. W. Horton, *Phys. Rep.* **192**, 1 (1990).
9. M. Tabor, *Chaos and Integrability in Nonlinear Dynamics* (Wiley, New York, 1989); M. V. Berry, *Am. Inst. Phys. Conf. Proc.* **46**, 16 (1978); P. Holmes, *Phys. Rep.* **193**, 137 (1990).
10. C. Eckart, *J. Mar. Res.* **7**, 265 (1948).
11. P. Welander, *Tellus* **7**, 141 (1955); H. Aref, *Phys. Fluids A* **3**, 1009 (1991).
12. J. M. Ottino, L. W. Leong, L. H. Rising, P. D. Swanson, *Nature* **333**, 419 (1988).
13. L. R. M. Maas, *Dtsch. Hydrogr. Z.* **42**, 111 (1989).
14. R. Pasmanter, in *Physical Processes in Estuaries*, J. Dronkers and W. Van Leussen, Eds. (Springer-Verlag, Heidelberg, 1988), pp. 42–52.
15. H. Ridderinkhof and J. T. F. Zimmerman, in *Residual Currents and Long Term Transport*, vol. 38 of *Coastal and Estuarine Studies*, R. T. Cheng, Ed. (Springer-Verlag, New York, 1990), pp. 194–209; R. P. Signell and W. R. Geyer, *ibid.*, pp. 210–222.
16. H. Aref, *J. Fluid Mech.* **143**, 1 (1984).
17. W. L. Chien, H. Rising, J. M. Ottino, *ibid.* **170**, 355 (1986); D. V. Khakhar, H. Rising, J. M. Ottino, *ibid.* **172**, 419 (1986).
18. A. L. Bertozzi, *SIAM J. Math. Anal.* **19**, 1271 (1988); J. B. Weiss and E. Knobloch, *Phys. Rev. A* **40**, 2579 (1989); S. M. Cox *et al.*, *J. Fluid Mech.* **214**, 517 (1990); R. T. Pierrehumbert, *Geophys. Astrophys. Fluid Dyn.* **58**, 285 (1991).
19. For a more general review of the physical properties of the western Dutch Wadden Sea, see H. Postma, *Arch. Neerl. Zool.* **10**, 405 (1954); J. T. F. Zimmerman, *Neth. J. Sea Res.* **10**, 149 (1976).
20. Actually the tide is a quasi-periodic signal, even if, as in the Wadden Sea, it is primarily semidiurnal. The basic quasi-periodicity is the spring-to-neap tidal cycle because of the superposition of the lunar and solar semidiurnal tides. Aperiodic components may also be present because of wind forcing, although these are weak even compared to the tide-induced residual currents. Thus, with a strict periodicity of the principal semidiurnal lunar tide, M_2 in our model runs, we implicitly assume that this component dominates all dispersion processes in the area and that the presence of other components in the semidiurnal frequency window do not quantitatively affect the results of chaotic stirring. The latter assumption is certainly not trivial; see D. Beigie, A. Leonard, S. Wiggins, *Nonlinearity* **4**, 775 (1991).
21. H. Ridderinkhof, *Neth. J. Sea Res.* **24**, 9 (1989); _____ and J. T. F. Zimmerman, in *Residual Currents and Long Term Transport*, vol. 38 of *Coastal and Estuarine Studies*, R. T. Cheng, Ed. (Springer-Verlag, New York, 1990), pp. 93–104.
22. J. T. F. Zimmerman, *Neth. J. Sea Res.* **8**, 126 (1974).
23. The equations are made dimensionless by use of the length scale of the eddy lattice as the unit for the coordinates (x,y) and the oscillation period as the time unit.
24. Substituting Eq. 4 in Eqs. 1 and 2 and introducing the coordinate transformation $\xi = x + y$, $\vartheta = x - y$ gives

$$\dot{\xi} = \lambda T(t) + \lambda\nu\,[1 + T(t)]\sin(\pi\vartheta)$$
$$\dot{\vartheta} = \lambda T(t) + \lambda\nu\,[1 + T(t)]\sin(\pi\xi)$$

This system is reduced to a piece-wise linear system by substitution of $T(t) = 1$ $(0 < t \leq 0.5)$, $T(t) = -1$ $(0.5 < t \leq 1)$ and replacment of $\sin(\pi\xi)$ with the sawtooth function $X(\xi)$, with $X = 2\xi$ $(-0.5 < \xi \leq 0.5)$, $X = -2(\xi - 1)$ $(0.5 < \xi \leq 1.5)$, $X = 2(\xi - 2)$ $(1.5 < \xi \leq 2.5)$, and $\sin(\pi\vartheta)$ with a function $Y(\vartheta)$ with the same structure as $X(\xi)$. The result reads

$$\dot{\xi} = a_1\vartheta + c_1,\ \dot{\vartheta} = b_1\xi + d_1$$

in which the constants (a_i, b_i, c_i, d_i) differ for each quadrant of a circulation cell and for each half of the oscillation period. The particle trajectory can then be constructed by a simple analytical integration until it reaches the boundary of a quadrant, the end of a tidal half cycle, or both. A sequence of these integrations over a full cycle gives the particle position after one tidal period for each specified initial position. In fact, this is a mapping, but the ultimate form of the map is extremely cumbersome and therefore not reproduced here.
25. Terminology introduced by M. V. Berry and colleagues [*Ann. Phys. N.Y.* **122**, 26 (1979)].
26. V. Merlo, M. Pettini, A. Vulpiani, *Lett. Nuovo Cim.* **44**, 163 (1985); I. S. Aranson, M. I. Rabinovich, L. S. Tsimring, *Phys. Lett. A* **151**, 523 (1990).
27. J. T. F. Zimmerman, *Deep Sea Res.* **26**, 505 (1979).
28. E. Ott and T. M. Antonsen, Jr., *Phys. Rev. A* **39**, 3660 (1989).
29. J. W. Talbot and G. A. Talbot, *Rapp. P.-V. Reun. Cons. Int. Explor. Mer* **167**, 93 (1974).
30. K. F. Bowden and M. R. Howe, *J. Fluid Mech.* **17**, 271 (1963).
31. V. Rom-Kedar, *Physica D* **43**, 229 (1990); _____, A. Leonard, S. Wiggins, *J. Fluid Mech.* **214**, 347 (1990); V. Rom-Kedar and S. Wiggins, *Arch. Ration. Mech. Anal.* **109**, 239 (1990); *Physica D* **51**, 248 (1991); S. Wiggins, *Chaotic Transport in Dynamical Systems* (Springer-Verlag, Berlin, 1992); S. C. Ryrie, *J. Fluid Mech.* **236**, 1 (1992).
32. H. Aref and S. W. Jones, *Phys. Fluids A* **1**, 470 (1989); S. W. Jones, *ibid.* **3**, 1081 (1991).
33. Unfortunately there are no reliable observations of tracer distributions in the Wadden Sea that indicate the presence of multiple maxima in dispersing clouds or of patches that suggest the presence of "islands" in the chaotic stirring process. However, many of the results presented in (*29*) do indeed show multiple maxima in artificial tracer experiments in similar tidal areas.
34. The numerical model used to simulate the quasi-2-D tidal velocity field [H. Ridderinkhof, *Neth. J. Sea Res.* **22**, 1 (1988)] uses an alternative direction-implicit method on a staggered grid [G. S. Stelling, *Commun. Rijkswaterstaat* **35**, 1 (1984)] to solve the nonlinear shallow-water equations. A grid size of 500 m and a time step of 150 s are used. These parameters are sufficient to reproduce the spatial structure of the 2-D, vertically averaged, tidal velocity field including the residual eddies. Trajectories of fluid particles are obtained by use of a second-order midpoint rule to integrate the Lagrangian velocity, which is evaluated with bilinear interpolation from surrounding grid points [H. Ridderinkhof, J. T. F. Zimmerman, M. E. Philippart, *Neth. J. Sea Res.* **25**, 331 (1990)].

35. We thank Rijkswaterstaat and the Institute for Computer-Integrated Manufacturing for the use of their extended system of computer programs for simulation of 2-D tidal flows (WAQUA). This is publication no. 37 of the Project "Ecological Research—North Sea and Wadden Sea."